IOP Conference Series: Earth and Environmental Science

PAPER • OPEN ACCESS

# Dynamic performance and sensitivity of grid-connected hydropower station under uncertain disturbance

To cite this article: Y Liu *et al* 2022 *IOP Conf. Ser.: Earth Environ. Sci.* **1079** 012113

# Dynamic performance and sensitivity of grid-connected hydropower station under uncertain disturbance

**Y Liu, W C Guo, R Cao, Z Chen and L Wang**

School of Civil and Hydraulic Engineering, Huazhong University of Science and Technology, Wuhan, 430074, China

Corresponding author: W C Guo, E-mail: wencheng@hust.edu.cn

**Abstract**. The grid-connected operating condition of hydropower station is a common operation mode to provide electric energy for the load side. This paper investigates the dynamic performance and sensitivity of grid-connected hydropower station (GCHS) under uncertain disturbance. Firstly, the nonlinear uncertain model of GCHS under uncertain disturbance is established. Then, the dynamic performance of GCHS is studied when the governor parameters change under certain step disturbance, periodic disturbance and uncertain random disturbance, respectively. Finally, based on the sensitivity index of the uncertain output obtained from the extended Fourier amplitude sensitivity test method, the sensitivity of the uncertain random disturbance at different input positions is studied. The results indicate that the GCHS under periodic disturbances or random disturbances have more complex dynamic performance than that under certain step disturbance. Under periodic disturbance, the forced oscillations and high frequency resonances are generated in dynamic response of GCHS. Under the uncertain random disturbance, the system of GCHS always presents random oscillation. The state variables $q_H$, z, $q_P$, $y$, $x_s$, $x_t$, and $\delta$ of GCHS are the most sensitive to uncertain disturbances, which are introduced at the generator or surge tank. The uncertain disturbances have significant interaction on the dynamic response of GCHS.

## 1. Introduction

As more and more new energy power with strong volatility, intermittency and randomness, such as wind power generation and photovoltaic power generation, are integrated into the power grid, the uncertainty of power grid becomes stronger [1,2]. Compared with traditional power grid, the structure of new power grid has changed significantly. It poses a huge challenge to the stable operation and control of the power system. Hydropower station can start or stop quickly and regulate flexibly. Then, the grid-connected hydropower station (GCHS) can be used as an important equipment for the peak-load shifting, frequency regulation services and emergency standby power supply in power system [1,3].

There are some previous researches on the operation and uncertainty sensitivity analysis of the GCHS, the representative papers are listed as follows: Liu et al. [1] establish a coupling mathematical model for grid-connected hydropower stations with surge tank, investigate the multi-frequency dynamic performance of hydropower plant under coupling effect of power grid and turbine regulating system with surge tank. Xu et al. [2] study the parametric uncertainty of hybrid power system model with solar-wind-hydro power, and quantify all the parameter's interaction contributions of the pumped storage station integrated to the hybrid power system with the EFAST method. Zhang et al. [4,5] establish a multi-frequency scale dynamic model of the hydraulic turbine regulating system by using the dynamic transfer coefficient in the form of periodic excitation to describe the dynamic characteristics of the turbine regulating system. Through numerical simulation, it is found that the system has typical fast and slow dynamic characteristics, and the instability mechanism of the system is revealed with the excitation amplitude and frequency increasing. Zhang et al. [6] propose an analytical expression of hydraulic unbalanced force to connect the traditional model of hydropower regulation system and model of the mechanical subsystem. Then the overall coupled dynamic model of the system is constructed. The extended Fourier amplitude sensitivity test (EFAST) is used to analyze the sensitivity of the typical parameters of the complex hydropower system model. Yuan et al. [7] establish a nonlinear uncertain dynamic model of integrated hydraulic turbine regulating system, and propose a novel approach to load frequency control for hydraulic turbine regulating system. According to previous researches, the uncertain dynamic characteristics of GCHS have hardly been studied. The purpose of this paper is to study dynamic performance and sensitivity of GCHS under uncertain disturbance. In view of that, the novelty and innovation of this paper are: (1) Establish the nonlinear uncertainty mathematical model of GCHS. (2) Reveal the influence of various disturbances on the dynamic performance of the GCHS. (3) Analyze influence of uncertain disturbances on the output of dynamic response of the GCHS state variables, reveal the effect degree of each uncertain disturbance on the output state variables. The structure of paper is as follows. In Section 2, the nonlinear uncertainty model of GCHS considering the throttling orifice head loss of surge tank is established, where, the throttling orifice of surge tank is an orifice at the bottom of surge tank, whose section area is smaller than the section area of the headrace tunnel. In Section 3, the dynamic performance of GCHS is studied with the governor parameters change under the certain load step disturbance, periodic disturbance and uncertain random disturbance, respectively. In Section 4, the main and total sensitivities of the uncertain output of the system for the uncertain disturbances are studied by EFAST. In Section 5, the conclusions are summarized.

## 2. Mathematical formulation and research methods

Based on the certain model considering throttling orifice head loss of surge tank, the model of GCHS under uncertain disturbance is established in this section. The GCHS is composed of headrace tunnel, surge tank, penstock, hydro-turbine, governor, generator and power grid. The basic equations for each part are presented as follows. It should be noted that the explanations for variables and parameters are presented in Appendix.

### *2.1. Mathematical model of GCHS under uncertain disturbance*

Equation of headrace tunnel [8]:

$$T_{wH0}\frac{\mathrm{d}q_H}{\mathrm{d}t} = z - \frac{2h_{H0}}{H_0}q_H - \frac{\alpha_T Q_0^2}{H_0}\left(q_P - q_H\right)^2 \tag{1}$$

Equation of surge tank [1]:

$$q_P = q_H + T_F\frac{\mathrm{d}z}{\mathrm{d}t} \tag{2}$$

Equation of penstock [8]:

$$T_{wP0}\frac{\mathrm{d}q_P}{\mathrm{d}t} = -z - h - \frac{2h_{P0}}{H_0}q_P - \frac{\alpha_T Q_0^2}{H_0}\left(q_P - q_H\right)^2 \tag{3}$$

Equation of turbine [1]:

$$m_t = e_h h + e_x x_t + e_y y\ ,\ q_P = e_{qh}h + e_{qx}x_t + e_{qy}y \tag{4}$$

Equation of governor [1]:

$$\frac{\mathrm{d}y}{\mathrm{d}t} = -K_p\frac{\mathrm{d}x_t}{\mathrm{d}t} - K_i x_t \tag{5}$$

Equation of generator [1]:

$$\begin{cases} \dfrac{\mathrm{d}\delta}{\mathrm{d}t} = 2\pi f_r \left(x_t - x_s\right) \\ T_a \dfrac{\mathrm{d}x_t}{\mathrm{d}t} = m_t - e_g x_t - \left[ \dfrac{E'V_t}{x'_d} \sin\delta + \dfrac{V_t^2}{2} \dfrac{x'_d - x_q}{x'_d x_q} \sin 2\delta - \left( \dfrac{E'V_t}{x'_d} \sin\delta_0 + \dfrac{V_t^2}{2} \dfrac{x'_d - x_q}{x'_d x_q} \sin 2\delta_0 \right) \right] - D_a \left(x_t - x_s\right) - m_g \end{cases} \tag{6}$$

Equation of power grid [1,3,9]:

$$\begin{cases} \dfrac{\mathrm{d}x_s}{\mathrm{d}t} = \dfrac{1}{T_s} \left\{ \begin{array}{l} B\left[ \dfrac{E'V_t}{x'_d} \sin\delta + \dfrac{V_t^2}{2} \dfrac{x'_d - x_q}{x'_d x_q} \sin 2\delta - \left( \dfrac{E'V_t}{x'_d} \sin\delta_0 + \dfrac{V_t^2}{2} \dfrac{x'_d - x_q}{x'_d x_q} \sin 2\delta_0 \right) \right] + BD_a x_t \\ -\left(BD_a + D_s\right) x_s - \dfrac{\xi}{T_g R_g} \end{array} \right\} \\ \dfrac{\mathrm{d}\xi}{\mathrm{d}t} = x_s - \dfrac{1}{T_g} \xi \end{cases} \tag{7}$$

In the actual operation processes, the uncertain disturbance inputs are usually step, cyclic or random. Therefore, the uncertainty of the system can be introduced into each order of the state equations (1), (2), (3), (5), (6) and (7) by uncertain terms $d_i$ ($i$ =1, 2 ,3, ⋯ ,8). Uncertain terms are expressed in three ways: (1) step disturbance, $d_i$ =const. (2) periodic disturbance, $d_i = A_i \sin(w_i t)$. (3) random disturbance, $d_i$ =$A_i$[2rand(1)-1], where $w_i$=2π/$T_i$, $T_i$ and $A_i$ represent the amplitude and period of the $i$-th disturbance. Then, the equation (8) of GCHS under uncertain disturbance can be obtained as follows by simultaneous equations (1), (2), (3), (4), (5), (6) and (7).

$$\begin{cases} \dot{q}_H = \dfrac{1}{T_{wH0}} \left( -\dfrac{2h_{H0}}{H_0} q_H + z - \dfrac{\alpha_T Q_0^2}{H_0} \left(q_P - q_H\right)^2 \right) + d_1 \\ \dot{z} = \dfrac{1}{T_F} \left(-q_H + q_P\right) + d_2 \\ \dot{q}_P = \dfrac{1}{T_{wP0}} \left[ -\left( \dfrac{2h_{P0}}{H_0} + \dfrac{1}{e_{qh}} \right) q_P - z + \dfrac{1}{e_{qh}} \left(e_{qx} x_t + e_{qy} y\right) - \dfrac{\alpha_T Q_0^2}{H_0} \left(q_P - q_H\right)^2 \right] + d_3 \\ \dot{x}_t = \dfrac{e_h}{T_a e_{qh}} q_P + \dfrac{1}{T_a} \left( e_x - e_g - D_a - \dfrac{e_h e_{qx}}{e_{qh}} \right) x_t + \dfrac{1}{T_a} \left( e_y - \dfrac{e_h e_{qy}}{e_{qh}} \right) y + \dfrac{D_a}{T_a} x_s \\ \quad - \dfrac{1}{T_a} \left[ \left( \dfrac{E'V_t}{x'_d} \sin\delta + \dfrac{V_t^2}{2} \dfrac{x'_d - x_q}{x'_d x_q} \sin 2\delta \right) - \left( \dfrac{E'V_t}{x'_d} \sin\delta_0 + \dfrac{V_t^2}{2} \dfrac{x'_d - x_q}{x'_d x_q} \sin 2\delta_0 \right) \right] - \dfrac{m_g}{T_a} + d_4 \\ \dot{y} = -\dfrac{K_p e_h}{T_a e_{qh}} q_P - \dfrac{K_p}{T_a} \left( e_x - e_g - D_a - \dfrac{e_h e_{qx}}{e_{qh}} + \dfrac{T_a K_i}{K_p} \right) x_t - \dfrac{K_p}{T_a} \left( e_y - \dfrac{e_h e_{qy}}{e_{qh}} \right) y - \dfrac{K_p D_a}{T_a} x_s \\ \quad + \dfrac{K_p}{T_a} \left[ \left( \dfrac{E'V_t}{x'_d} \sin\delta + \dfrac{V_t^2}{2} \dfrac{x'_d - x_q}{x'_d x_q} \sin 2\delta \right) - \left( \dfrac{E'V_t}{x'_d} \sin\delta_0 + \dfrac{V_t^2}{2} \dfrac{x'_d - x_q}{x'_d x_q} \sin 2\delta_0 \right) \right] + \dfrac{K_p}{T_a} m_g + d_5 \\ \dot{x}_s = \dfrac{1}{T_s} \left[ \begin{array}{l} BD_a x_t - \left(BD_a + D_s\right) x_s + B\left( \dfrac{E'V_t}{x'_d} \sin\delta + \dfrac{V_t^2}{2} \dfrac{x'_d - x_q}{x'_d x_q} \sin 2\delta \right) \\ -B\left( \dfrac{E'V_t}{x'_d} \sin\delta_0 + \dfrac{V_t^2}{2} \dfrac{x'_d - x_q}{x'_d x_q} \sin 2\delta_0 \right) - \dfrac{1}{T_g R_g} \xi \end{array} \right] + d_6 \\ \dot{\delta} = 2\pi f_r \left(x_t - x_s\right) + d_7 \\ \dot{\xi} = x_s - \dfrac{1}{T_g} \xi + d_8 \end{cases} \tag{8}$$

### *2.2. Research methods*

*2.2.1. Analysis method of system dynamic performance.* (1) The dynamic response of the GCHS is obtained by solving equation (8) with the function of ode45 in Matlab [10], under initial condition

$\boldsymbol{x}_0 = \left(q_{H0}, z_0, q_{P0}, x_{t0}, y_0, x_{s0}, \delta_0, \xi_0\right)^T$. (2) Bifurcation diagram reflects the dynamic behavior of GCHS with the change of parameters, and is drawn by local maximum method [11]. (3) Chaos dynamics is represented by Lyapunov exponents (LEs) of positive value which reflects the strength of the system's chaotic effect [11]. (4) The dynamic response of the GCHS state variables are processed by fast Fourier transform (FFT) to draw the spectrum diagram [12]. The more complex the spectrum component, the more complex the dynamic behavior of the system.

*2.2.2. Method of sensitivity analysis.* The extended Fourier amplitude test (EFAST) [13, 14] is used to analyze the sensitivity of dynamic characteristic output of each state variables to uncertain disturbances. The main sensitivity index only represents the sensitivity of the one parameter's direct effect on the output variance of GCHS. The total sensitivity index is the sum of the direct contribution of one parameter plus the indirect contribution from the interaction with other parameters [13,14]. Main sensitivity index $S_i$ and total sensitivity index $S_{Ti}$ of $P_i$ can be calculated as follows [13,14].

$$S_i = \frac{V_i}{V},\ S_{Ti} = \frac{V - V_{-i}}{V} \tag{9}$$

where $V_i$ is the variance of model results caused by the $P_i$. In this section, the variance has its specific definition and calculation method in the EFAST method [13, 14], and the variance is calculated according to the spectrum of the defined Fourier series. And $V_{-i}$ is the sum of the variances of all parameters excluding $P_i$, in which $i$=1, 2 , 3, ⋯, 8 is the $i$-th parameter. Based on EFAST method [13, 14], dynamic response output of GCHS system under uncertain disturbance can be written as a function $f(s,t)$ of $s$ and $t$, where $s$ is common variables of $P_i$. Sensitivity indexes of this research are defined as follows. (1) The maximal deviation value (MDV) is an important index for safe of GCHS, denoted as $f_{MDV}(s,t)$. MDV can represents the farthest value of the system from the initial value, which reflects the safety of the GCHS. The larger the MDV, the smaller the safety margin of the system. The $S_i$ and $S_{Ti}$ of $f_{MDV}(s,t)$ are denoted as $MDVS_i$ and $MDVS_{Ti}$. (2) The $S_i$ and $S_{Ti}$ are the indexes corresponding to any time $t$, i.e. $S_i = S_i(t)$ and $S_{Ti} = S_{Ti}(t)$. The average sensitivity indexes for $S_i$ and $S_{Ti}$ are denoted as $ATS_i$ and $ATS_{Ti}$ in the time interval $(t_1, t_2)$, respectively. In the time interval $(t_1, t_2)$, $ATS_i$ and $ATS_{Ti}$ are calculated as follows, where $D$ is time step. In this paper, $D$ =0.1 s.

$$ATS_i = \frac{\sum_{t_1}^{t_2} S_i(t)}{(t_2 - t_1)D^{-1}+1},\ ATS_{Ti} = \frac{\sum_{t_1}^{t_2} S_{Ti}(t)}{(t_2 - t_1)D^{-1}+1} \tag{10}$$

## 3. Dynamic performance of GCHS under uncertain disturbance

In Section 2, the model of GCHS under uncertain disturbance is established. Different uncertain disturbances have great effect on the dynamic performance of GCHS. In this section, two kinds of disturbance are selected to act on the certain system to reveal the effect of different disturbances inputs on the dynamic performance of GCHS. The dynamic performance of GCHS is studied by bifurcation diagram, LEs, and spectrogram. When $K_p$ and $K_i$ change, the dynamic responses are calculated under the certain load step disturbance $m_g$, periodic disturbance, and uncertain random disturbance, respectively. The three situations correspond to Situation 1, Situation 2 and Situation 3. The model under Situation 1 is also called the certain model. And the basic parameter values for the selected engineering example of GCHS are listed in table 1. The selected types of disturbances are listed in table 2. It should be noted that the explanations for variables and parameters are presented in Appendix.

### *3.1. Analysis of bifurcation diagram and Lyapulov exponents*

In this section, the bifurcation diagram and the maximum LEs (Max LEs) are used to describe the dynamic performance of the GCHS with the change of governor parameters. In the actual operation of hydropower station, the parameters of the governor are relatively easy to adjust to improve the quality of the dynamic response of the system, and have a greater impact on the stability of the system. Based on the above consideration, $K_i$ and $K_p$ are selected as the abscissa. Based on the equation (8), basic parameters in table 1, types of disturbances in table 2 and the GCHS initial value (0,0,0,0,0,0,0.461, 0), the dynamic response of $x_t$ can be calculated when the governor parameter $K_p$ =3 and $K_i$ varies in 0-4.0 $s^{-1}$. Then, the bifurcation diagram can be drawn and Max LEs can be calculated for Situation 1, Situation 2 and Situation 3, respectively. Results are shown in figure 1(a). When $K_i$ =2.243 $s^{-1}$ and $K_p$ varies in 0-10.8, the results are shown in figure 1(b). $x_{t\text{-}0}$, $x_{t\text{-}c}$ and $x_{t\text{-}r}$ represent the dynamic response of the rotational speed deviation of the Situation 1, Situation 2 and Situation 3 in figure 1, respectively.

**Table 1.** Basic parameter values for the selected engineering example of GCHS.

| Symbol | Unit | Value | Symbol | Unit | Value | Symbol | Unit | Value | Symbol | Unit | Value |
|---|---|---|---|---|---|---|---|---|---|---|---|
| $H_0$ | m | 89 | $T_F$ | s | 280 | $T_a$ | s | 10 | $f_r$ | Hz | 50 |
| $Q_0$ | $m^3 \cdot s^{-1}$ | 39 | $e_h$ | p.u | 1.5 | $D_a$ | p.u | 17 | $B$ | p.u | 0.1 |
| $\alpha_T$ | $s^2 \cdot m^{-5}$ | 0.004 | $e_x$ | p.u | -1 | $x'_d$ | p.u | 1.232 | $D_s$ | p.u | 0.4 |
| $T_{WH0}$ | s | 23.84 | $e_y$ | p.u | 1 | $E'$ | p.u | 1.978 | $T_s$ | s | 40 |
| $h_{H0}$ | m | 7.57 | $e_{qh}$ | p.u | 0.5 | $x_q$ | p.u | 0.645 | $R_g$ | p.u | 0.2 |
| $T_{WP0}$ | s | 2.33 | $e_{qx}$ | p.u | 0 | $V_t$ | p.u | 1 | $T_g$ | s | 40 |
| $h_{P0}$ | m | 5.53 | $e_{qy}$ | p.u | 1 | $\delta_0$ | rad | 0.461 | $m_g$ | p.u | -0.1 |

**Table 2.** Selected types of disturbances.

| $d_i$ | Situation 1 Certain model | Situation 2 Periodic disturbance | Situation 3 Random disturbance | $d_i$ | Situation 1 Certain model | Situation 2 Periodic disturbance | Situation 3 Random disturbance |
|---|---|---|---|---|---|---|---|
| $d_1$ | 0 | $0.001\sin(t)$ | $0.001\left[2\text{rand}(1)-1\right]$ | $d_5$ | 0 | $-0.001\sin(t)$ | $-0.001\left[2\text{rand}(1)-1\right]$ |
| $d_2$ | 0 | $-0.001\sin(2t)$ | $-0.001\left[2\text{rand}(1)-1\right]$ | $d_6$ | 0 | $0.001\sin(0.5t)$ | $0.001\left[2\text{rand}(1)-1\right]$ |
| $d_3$ | 0 | $0.001\sin(t)$ | $0.001\left[2\text{rand}(1)-1\right]$ | $d_7$ | 0 | $0.001\cos(t)$ | $0.001\left[2\text{rand}(1)-1\right]$ |
| $d_4$ | 0 | $-0.001\sin(0.5t)$ | $-0.001\left[2\text{rand}(1)-1\right]$ | $d_8$ | 0 | $-0.001\sin(t)$ | $-0.001\left[2\text{rand}(1)-1\right]$ |

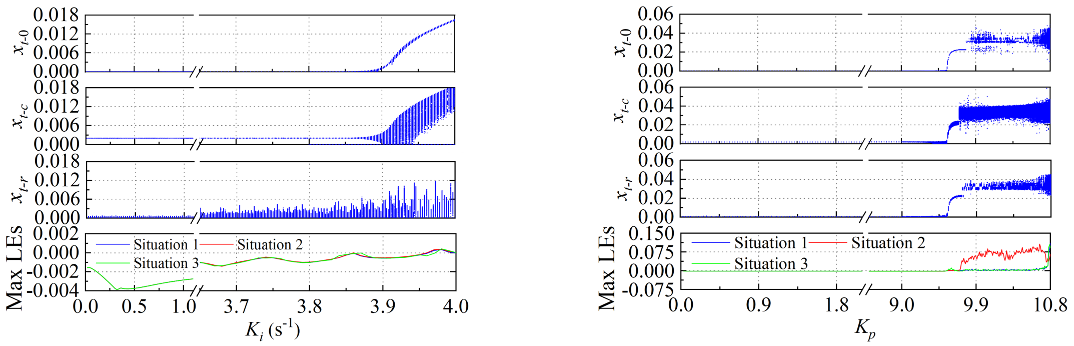


(a) (b)

**Figure 1.** Bifurcation diagrams and Max LEs of state variable $x_t$ with governor parameters change under three situations, (a) $K_p$ =3 and $K_i$ =0 $s^{-1}$-4.0 $s^{-1}$, (b) $K_p$ =0-10.8 and $K_i$ =2.243 $s^{-1}$.

Figure 1 shows that: (1) According to figure 1(a), when $K_p$ =3 and $K_i$ varies in 0$s^{-1}$-4.0 $s^{-1}$, the three kinds of situations experience two states of motion. The first stage, when $K_i$ varies in 0$s^{-1}$-3.905 $s^{-1}$, the Situation 1 is stable eventually, and $x_{t\text{-}0}$ can converge to a fixed value $x_t$ =0. The Situation 2 under the periodic disturbance is in a state with forced continuous constant amplitude oscillation eventually, and amplitude of $x_{t\text{-}c}$ is 0.002, and can't converge to a fixed value. The second stage, when $K_i$ varies in 3.905 $s^{-1}$-4 $s^{-1}$, Situation 1 and Situation 2 are in a continuous oscillatory state with increasing amplitude of $x_t$. Compared to Situation 1, the positions of points on the bifurcation diagram are more dispersed for Situation 2. For Situation 3, the boundaries of first stage and the second stage are not as clear as Situation 1 and Situation 2. When $K_i$ is small, the GCHS under Situations 3 has continuous random oscillation in a small bounded range, and can't converge to a fixed value. When $K_i$ is close to 4 s$^{-1}$, the $x_{t-r}$ of GCHS under Situations 3 is in a state of continuous random vibration with increasing amplitude, then $x_{t-r}$ is unstable eventually. The value of Max LEs increases as $K_i$ increases. When the $K_i$ increases, and reaches a certain value, the Max LEs of Situation 2 is greater than that of Situation 1, and the Max LEs of Situation 3 fluctuates up and down in Situation 1. (2) According to figure 1(b), when $K_i$ =2.243 s$^{-1}$ and $K_p$ varies in 0-10.8 s$^{-1}$, the $x_t$ of GCHS experiences three states of motion. The first stage: The $x_{t-0}$ of GCHS can finally stabilize to the equilibrium point $x_{t-0}$ =0 for Situation 1. The GCHS has a constant-amplitude oscillation which the amplitude of $x_{t-c}$ is 0.002 for Situation 2 eventually. The GCHS vibrates randomly in a small bounded range for Situation 3. The second stage, the amplitude of $x_t$ tends to increase as $K_p$ increases, the GCHS is in the critical region of complete instability for three situations. The third stage, the points on the bifurcation diagram become denser and denser with scattered points, in a state of random disorder and uncertain chaotic motion. All three situations enter the second stage at $K_p$ =9.55. Situation 1, Situation 2 and Situation 3 enter the third stage at 9.78, 9.70 and 9.74, respectively. For Max LEs, it is consistent with the previous bifurcation diagram analysis. The three stages correspond to Max LEs <0, Max LEs is almost equal to 0 and Max Les >0, respectively. That represents the process of the operating state of the GCHS from stable to chaotic. Compared with Situation 1 and Situation 3, the Max LEs of Situation 2 suddenly increases in the third stage, and is much larger than that of Situation 1 and Situation 3. It shows that the system under periodic disturbance is easier to enter the state of chaotic motion than the certain model and the model under uncertain random disturbance with the increase of $K_p$. In the second stage, Max LEs of Situation 3 is larger or smaller than Max LEs that of Situation 1. However, compared with Situation 2, the Situation 3 does not appear drastic mutation. Due to the existence of periodic disturbances and uncertain random disturbances, the vibration of the GCHS becomes more and more complicated with the increase of the governor parameters. The bifurcation diagram of the GCHS is not converging to a fixed value or oscillating with a constant amplitude. The dynamic response of the system has multiple extreme values, the bifurcation diagram of the GCHS has multiple points for a set of governor parameters.

### *3.2. Analysis of dynamic response and frequency components*

Corresponding to Section 3.1, in this section, the state points $S_1$ ($K_p$=3, $K_i$=2.243 s$^{-1}$), $S_2$ ($K_p$=3, $K_i$=3.95 s$^{-1}$), $S_3$ ($K_p$=9.6, $K_i$=2.243 s$^{-1}$) and $S_4$ ($K_p$=10, $K_i$=2.243 s$^{-1}$) are selectd to substitute into Situation 1, Situation 2 and Situation 3. Then, the dynamic response of $x_t$ is calculated and the spectrums of $x_t$ is obtained by FFT. The dynamic response and spectrums of the $x_{t-0}$, $x_{t-c}$, $x_{t-r}$ for $S_1$, $S_2$, $S_3$ and $S_4$ are shown in figure 2(a)- 2(d) and figure 2(e)- 2(h), respectively. The $A(x_t)$ represents the amplitude of $x_t$.

Figure 2 shows that there are obvious phenomena of oscillation superposition under state points $S_1$, $S_2$, $S_3$ and $S_4$. Under $S_1$, the $x_{t-0}$ of Situation 1 converges to the equilibrium point $x_{t-0}$=0 after multiple oscillations. There are three basic frequency oscillations in system, i.e. subwave-1=0.0016Hz, subwave-2 =0.0138 Hz and subwave-3 =1.2532 Hz. The $x_{t-c}$ of Situation 2 enters the constant-amplitude oscillation eventually. Compared with the Situation 1, the system under Situation 2 has an forced oscillation with a frequency of 0.0796 Hz, which is denoted as subwave-c. The $x_{t-r}$ of Situation 3 is in a continuous random oscillation, and the three frequency spectra are not smooth in spectrogram. Under $S_2$, the $x_{t-0}$ of Situation 1 enters the state of oscillation of constant amplitude after the oscillation of gradually increasing amplitude. For Situation 2, the $x_{t-c}$ enters a continuous oscillation state superimposed by multiple frequency waves. Moreover, the spectral distribution of subwave-3 region is more dispersed than that of the Situation 1. For Situation 3, $x_{t-r}$ finally enters a continuous random oscillation state, and there are vibration increase or decrease in the dynamic response of the same system. The spectrum of subwave-1 and subwave-3 are not clear. Under $S_3$, $x_{t-0}$ of Situation 1 enters the state of constant amplitude oscillation after the stage of amplitude increasing oscillation, and subwave-3 has a harmonic of 2.088Hz. The $x_{t-c}$ of Situation 2 has subwave-c =0.0796Hz, and there are more than two frequencies in the spectrum near subwave-3 and its harmonics. The $x_{t-r}$ of the GCHS under Situation 3 is consistent with Situation 1, but the three spectra are not clear. Under S$_4$, the $x_t$ of the three situations finally enter the chaotic vibration state with no clear rules. For Situation 1, the separation of three basic subwaves are not obvious. However, there are waves of

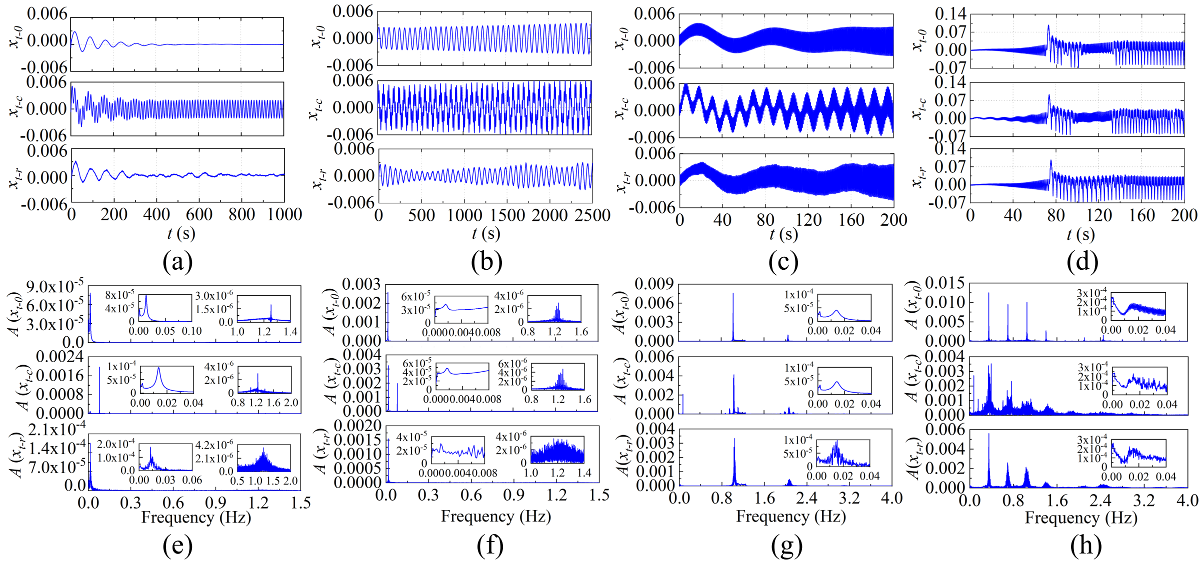

**Figure 2.** Dynamic response and spectrum diagram of state variables $x_{t\text{-}0}$, $x_{t\text{-}c}$, $x_{t\text{-}r}$ for three situations under state points $S_1$, $S_2$, $S_3$ and $S_4$, (a) Dynamic response of $x_{t\text{-}0}$, $x_{t\text{-}c}$, $x_{t\text{-}r}$ under $S_1$, (b) Dynamic response of $x_{t\text{-}0}$, $x_{t\text{-}c}$, $x_{t\text{-}r}$ under $S_2$, (c) Dynamic response of $x_{t\text{-}0}$, $x_{t\text{-}c}$, $x_{t\text{-}r}$ under $S_3$, (d) Dynamic response of $x_{t\text{-}0}$, $x_{t\text{-}c}$, $x_{t\text{-}r}$ under $S_4$, (e) Spectrum diagram of $x_{t\text{-}0}$, $x_{t\text{-}c}$, $x_{t\text{-}r}$ under $S_1$, (f) Spectrum diagram of $x_{t\text{-}0}$, $x_{t\text{-}c}$, $x_{t\text{-}r}$ under $S_2$, (g) Spectrum diagram of $x_{t\text{-}0}$, $x_{t\text{-}c}$, $x_{t\text{-}r}$ under $S_3$, (h) Spectrum diagram of $x_{t\text{-}0}$, $x_{t\text{-}c}$, $x_{t\text{-}r}$ under $S_4$.

0.3502 Hz and its multiple high frequency harmonics. For Situation 2, the system has a forced oscillation with a frequency of subwave-c =0.0796 Hz and a number of its multiple high-frequency harmonics. From the whole spectrogram, the spectrum of the system for Situation 2 is almost stacked together, and only some very prominent main oscillations are visible. So under $S_4$, the periodic disturbance makes the dynamic performance of the system more complicated. The dynamic response of the system under random disturbance has high frequency harmonics and multiple frequencies harmonics, for which the basic frequency is 0.3502 Hz. Compared with the GCHS under periodic disturbance, its influence on the main oscillation is smaller. Compared with the certain model, it is more uncertain. The GCHS under random or periodic disturbances can't converge to a fixed point under any state points. The GCHS always has a random or continuous oscillation of multiple fluctuations, because random disturbances and periodic disturbances are time-varying when calculating the dynamic response of the GCHS. According to the previous analysis, the following conclusions can be obtained. When $K_p$ and $K_i$ are in a relatively stable region, the certain model can stabilize to equilibrium point $x_{t\text{-}0}$ =0. While the GCHS under periodic disturbance has continuous constant-amplitude oscillation and cannot stabilize at equilibrium point eventually. The oscillation of GCHS under random disturbance is reduced and has a continuous random vibration in a small bounded range eventually. When $K_p$ and $K_i$ are in the critical region, the certain model has a constant amplitude oscillation, while the other two models continue to vibrate under the dominance of the base frequency of the certain models. There is little difference among the three models for the critical stable point. The model under periodic disturbance enters the chaotic region is earlier than the certain model and the model under random disturbance with the increase of the governor parameters. The model under the periodic disturbance not only introduces the natural frequency but also generates multiple high frequency harmonics of the disturbance, and induces the vibration of other frequencies.

## 4. Sensitivity of GCHS under uncertain disturbance

In Section 3, the effects of different disturbances on the dynamic performance of the GCHS have been analyzed. In this section, the uncertain disturbance is simulated as step disturbance on equation (8). It is assumed that the uncertain disturbances of equation (8) are determined in the initial condition, the disturbances do not change over time in process of calculating the dynamic response. Firstly, the $MDVS_i$ and $MDVS_{Ti}$ of $f_{MDV}(s,t)$ are calculated and analyzed. Then, the $ATS_i$ and $ATS_{Ti}$ of $f(s,t)$ in time intervals are calculated and analyzed. In equation (8), $d_i = U_{Di}$ represents the uncertain disturbance acting on $i$-th order state term. The uncertain disturbance sets are calculated using normally distributed samples. For that, the mean value is $\mu$ =0.01 and the standard deviation is $\sigma$=0.001/3. For the uncertain disturbance sets, choose constant $M$ =6, characteristic frequency $\{\omega_i\}'$ ={1, 2, 3, 4, 5, 6, 7}, $\omega_i$=2M·max($\{\omega_i\}'$) =84, resampling times $N_r$ =6, number of parameters $n$ =8, the calculation cost is $C = N_r[n(2M\omega_{\max}+1)]$ =48432 times. The uncertain model output is calculated by substituting the basic parameter values for the selected engineering example of GCHS in table 1 and the uncertain disturbance sets into equation (8), where $\alpha_T$ =0.0004 s$^2$ m$^{-5}$, $K_p$ =1 and $K_i$ =1 s$^{-1}$ in this section. Then, the sensitivity indexes of $f_{MDV}(s,t)$ to uncertain disturbances are calculated by EFAST method, the result is shown in figure 3. And the average sensitivity indexes of the value of $f(s,t)$ output in time interval (0.1 s, 3000 s) to uncertain disturbances is shown in figure 4. $S_i$ >0.05 and $S_{Ti}$ >0.1 are regarded as the standard to judge whether sensitivity index is sensitive or not. In table 3 and table 4, the sensitivity indexes greater than the sensitivity standard are marked in bold.

### 4.1. Analysis of mian sensitivity index and total sensitivity index of $f_{MDV}(s,t)$

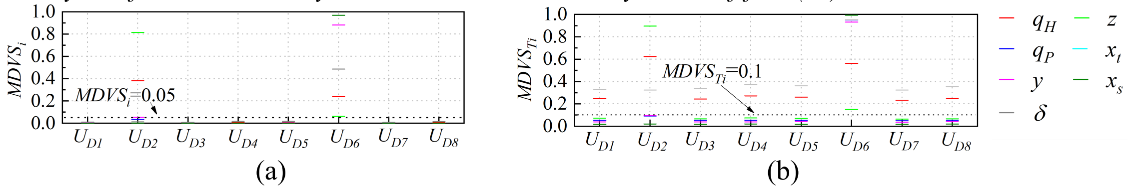


**Figure 3.** Sensitivity indexes of $f_{MDV}(s,t)$ to uncertain disturbances, (a) $MDVS_i$, (b) $MDVS_{Ti}$.

(1) According to the analysis in figure 3, the sorting of $MDVS_i$ and $MDVS_{Ti}$ corresponding to the dynamic response of $f(s,t)$ for state variables $q_H$, $z$, $q_P$, $y$, $x_s$, $x_t$ and $\delta$ are obtained as table 3.

**Table 3.** Sorting of $MDVS_i$ and $MDVS_{Ti}$ corresponding to the dynamic response of $f(s,t)$ for state variables $q_H$, $z$, $q_P$, $y$, $x_s$, $x_t$ and $\delta$.

| Variables | Sorting of $MDVS_i$ | Sorting of $MDVS_{Ti}$ |
|---|---|---|
| $q_H$ | **$U_{D2}$>$U_{D6}$**>$U_{D1}$>$U_{D4}$>$U_{D3}$>$U_{D7}$>$U_{D8}$>$U_{D5}$ | **$U_{D2}$>$U_{D6}$>$U_{D4}$>$U_{D5}$>$U_{D8}$>$U_{D1}$>$U_{D3}$>$U_{D7}$** |
| $z$ | **$U_{D2}$>$U_{D6}$**>$U_{D1}$>$U_{D4}$>$U_{D3}$>$U_{D7}$>$U_{D8}$>$U_{D5}$ | **$U_{D2}$>$U_{D6}$**>$U_{D4}$>$U_{D1}$>$U_{D5}$>$U_{D8}$>$U_{D3}$>$U_{D7}$ |
| $q_P$ | **$U_{D6}$**>$U_{D2}$>$U_{D5}$>$U_{D8}$>$U_{D3}$>$U_{D1}$>$U_{D4}$>$U_{D7}$ | **$U_{D6}$>$U_{D2}$**>$U_{D8}$>$U_{D4}$>$U_{D1}$>$U_{D5}$>$U_{D3}$>$U_{D7}$ |
| $x_t$ | **$U_{D6}$**>$U_{D4}$>$U_{D2}$>$U_{D8}$>$U_{D5}$>$U_{D3}$>$U_{D1}$>$U_{D7}$ | **$U_{D6}$**>$U_{D2}$>$U_{D4}$>$U_{D8}$>$U_{D5}$>$U_{D3}$>$U_{D1}$>$U_{D7}$ |
| $y$ | **$U_{D6}$>$U_{D2}$**>$U_{D5}$>$U_{D8}$>$U_{D4}$>$U_{D3}$>$U_{D1}$>$U_{D7}$ | **$U_{D6}$>$U_{D2}$**>$U_{D5}$>$U_{D8}$>$U_{D4}$>$U_{D1}$>$U_{D3}$>$U_{D7}$ |
| $x_s$ | **$U_{D6}$**>$U_{D4}$>$U_{D2}$>$U_{D8}$>$U_{D5}$>$U_{D3}$>$U_{D1}$>$U_{D7}$ | **$U_{D6}$>$U_{D2}$**>$U_{D4}$>$U_{D8}$>$U_{D5}$>$U_{D3}$>$U_{D1}$>$U_{D7}$ |
| $\delta$ | **$U_{D6}$**>$U_{D4}$>$U_{D5}$>$U_{D8}$>$U_{D2}$>$U_{D1}$>$U_{D3}$>$U_{D7}$ | **$U_{D6}$>$U_{D4}$>$U_{D5}$>$U_{D8}$>$U_{D3}$>$U_{D1}$>$U_{D7}$>$U_{D2}$** |

(2) In terms of the $MDVS_i$, $q_H$ and $z$ are the most sensitive to $U_{D2}$, and sensitive to $U_{D6}$ secondly. The $q_P$, $y$, $x_s$, $x_t$ and $\delta$ are the most sensitive to $U_{D6}$. $q_P$ and $y$ are the second sensitive to $U_{D2}$, and the third sensitive to $U_{D5}$. $x_s$, $x_t$ and $\delta$ are the second sensitive to $U_{D4}$. In particular, the values of $MDVS_i$ of $q_P$, $y$, $x_s$ and $x_t$ to exceed 0.8. It shows that $U_{D6}$ has great direct contribution to $f_{MDV}(s,t)$ of $q_P$, $y$, $x_s$ and $x_t$.The $MDVS_{Ti}$ of each uncertainty disturbance of $q_H$ and $\delta$ are much larger than that of the $MDVS_i$, indicating that these state variables are more obviously affected by the interaction of various uncertain disturbances.

### 4.2. Analysis of average sensitivity indexes of $f(s,t)$ in time intervals

The $ATS_i$ and $ATS_{Ti}$ of dynamic response to uncertain disturbances reflect the effects of the overall level on the GCHS. The calculation results are shown in figure 4.

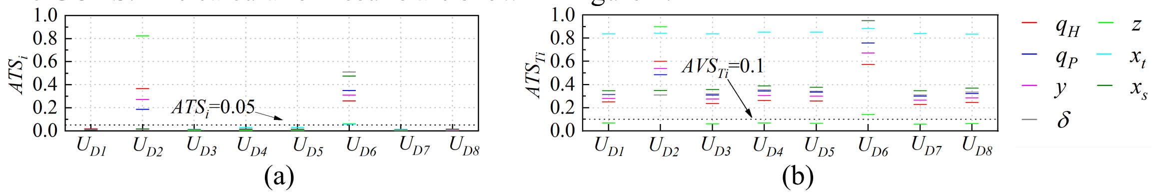


**Figure 4.** Average sensitivity indexes of $f(s,t)$ to uncertain disturbances in the time interval (0.1 s, 3000 s) , (a) $ATS_i$, (b) $ATS_{Ti}$.

(1) According to the analysis in figure 4, the sorting of $ATS_i$ and $ATS_{Ti}$ corresponding to the dynamic response of $f(s,t)$ for state variables $q_H$, $z$, $q_P$, $y$, $x_s$, $x_t$, and $\delta$ are obtained as table 4.

**Table 4.** Sorting of $ATS_i$ and $ATS_{Ti}$ corresponding to the dynamic response of $f(s,t)$ for state variables $q_H$, $z$, $q_P$, $y$, $x_s$, $x_t$ and $\delta$.

| Variables | Sorting of $ATS_i$ | Sorting of $ATS_{Ti}$ |
|---|---|---|
| $q_H$ | $\boldsymbol{U_{D2}}>\boldsymbol{U_{D6}}>U_{D1}>U_{D4}>U_{D3}>U_{D8}>U_{D5}>U_{D7}$ | $\boldsymbol{U_{D2}}>\boldsymbol{U_{D6}}>\boldsymbol{U_{D4}}>\boldsymbol{U_{D5}}>\boldsymbol{U_{D1}}>\boldsymbol{U_{D8}}>\boldsymbol{U_{D3}}>\boldsymbol{U_{D7}}$ |
| $z$ | $\boldsymbol{U_{D2}}>\boldsymbol{U_{D6}}>U_{D1}>U_{D4}>U_{D3}>U_{D8}>U_{D7}>U_{D5}$ | $\boldsymbol{U_{D2}}>\boldsymbol{U_{D6}}>U_{D1}>U_{D4}>U_{D5}>U_{D8}>U_{D3}>U_{D7}$ |
| $q_P$ | $\boldsymbol{U_{D6}}>\boldsymbol{U_{D2}}>U_{D1}>U_{D4}>U_{D3}>U_{D5}>U_{D8}>U_{D7}$ | $\boldsymbol{U_{D6}}>\boldsymbol{U_{D2}}>\boldsymbol{U_{D4}}>\boldsymbol{U_{D5}}>\boldsymbol{U_{D8}}>\boldsymbol{U_{D1}}>\boldsymbol{U_{D3}}>\boldsymbol{U_{D7}}$ |
| $x_t$ | $\boldsymbol{U_{D6}}>U_{D4}>U_{D5}>U_{D2}>U_{D8}>U_{D1}>U_{D3}>U_{D7}$ | $\boldsymbol{U_{D6}}>\boldsymbol{U_{D5}}>\boldsymbol{U_{D4}}>\boldsymbol{U_{D2}}>\boldsymbol{U_{D7}}>\boldsymbol{U_{D3}}>\boldsymbol{U_{D1}}>\boldsymbol{U_{D8}}$ |
| $y$ | $\boldsymbol{U_{D6}}>\boldsymbol{U_{D2}}>U_{D1}>U_{D4}>U_{D3}>U_{D5}>U_{D8}>U_{D7}$ | $\boldsymbol{U_{D6}}>\boldsymbol{U_{D2}}>\boldsymbol{U_{D4}}>\boldsymbol{U_{D5}}>\boldsymbol{U_{D8}}>\boldsymbol{U_{D1}}>\boldsymbol{U_{D3}}>\boldsymbol{U_{D7}}$ |
| $x_s$ | $\boldsymbol{U_{D6}}>U_{D2}>U_{D8}>U_{D4}>U_{D1}>U_{D5}>U_{D3}>U_{D7}$ | $\boldsymbol{U_{D6}}>\boldsymbol{U_{D4}}>\boldsymbol{U_{D5}}>\boldsymbol{U_{D8}}>\boldsymbol{U_{D3}}>\boldsymbol{U_{D2}}>\boldsymbol{U_{D1}}>\boldsymbol{U_{D7}}$ |
| $\delta$ | $\boldsymbol{U_{D6}}>U_{D4}>U_{D5}>U_{D8}>U_{D2}>U_{D1}>U_{D3}>U_{D7}$ | $\boldsymbol{U_{D6}}>\boldsymbol{U_{D4}}>\boldsymbol{U_{D5}}>\boldsymbol{U_{D8}}>\boldsymbol{U_{D3}}>\boldsymbol{U_{D1}}>\boldsymbol{U_{D2}}>\boldsymbol{U_{D7}}$ |

(2) In terms of the $ATS_i$, $q_H$ and $z$ are the most sensitive to $U_{D2}$, and sensitive to $U_{D6}$ secondly. $q_P$, $x_t$, $y$, $x_s$ and $\delta$ are the most sensitive to $U_{D6}$, and sensitive to $U_{D2}$ secondly. It is noted that the $ATS_i$ of $x_t$ is small, while the $ATS_{Ti}$ of $x_t$ is large, indicating that the interaction of uncertain disturbance at various points of GCHS on $x_t$ is obvious. Except for $z$, $ATS_{Ti}$ of other state variables are more larger than $ATS_i$. It shows that the effects of uncertain disturbances on the dynamic performance of CGHS have significant interactions.

The previous analysis in this section indicates that, the the stronger the state variable is coupled to the generator/the surge tank, the more sensitive it is to $U_{D6}/U_{D2}$. In order to obtain better dynamic performance, it is important to control the oscillation of water level of the surge tank and speed or load disturbance of generator.

## 5. Conclusions

The main conclusions are given as follows:

(1) By introducing uncertainty terms, the nonlinear uncertain model of GCHS considering the head loss of the surge tank throttling orifice is an eighth-order nonlinear state equation. The bifurcation diagram, LEs and frequency spectrum are used to describe and analyze the dynamic response of the GCHS well. EFAST is a practical approach to analyze the sensitivity of uncertain disturbances, which can quantitatively analyze the sensitivity of dynamic response of GCHS to uncertain disturbances.

(2) The GCHS under periodic disturbance not only introduces the frequency of the disturbance, but also generates it's multiple high frequency harmonics, and induces the vibration of other frequencies, with the increase of the governor parameters. The chaos of the GCHS under periodic disturbance is stronger than that the GCHS under random uncertain disturbance and the certain model. Under random uncertain disturbance, the GCHS always exists an unstable random oscillation. The trends of chaos under random uncertain disturbance is similar to the certain model.

(3) For the sensitivity indexes of $f_{MDV}(s,t)$ and average sensitivity indexes of $f(s,t)$ in time intervals, the $q_H$ and $z$ are the most sensitive to $U_{D2}$. The $q_P$, $y$, $x_s$, $x_t$ and $\delta$ are the most sensitive to $U_{D6}$. The $MDVS_{Ti}$ of $q_H$ and $\delta$ are much larger than that of the $MDVS_i$. Except for the $z$, the $ATS_{Ti}$ of other state variables are much larger than that of the $ATS_i$. The effects of uncertain disturbances on the dynamic performance of the GCHS have significant interactions. So, the stronger the state variable is coupled to the generator/the surge tank, the more sensitive it is to $U_{D6}/U_{D2}$. In order to obtain better dynamic performance, it is important to control the oscillation of water level of the surge tank and speed or load disturbance of generator.

## Acknowledgements

This work was supported by the National Natural Science Foundation of China (Project No. 51909097).

## Appendix

Nomenclature

| | | | |
|---|---|---|---|
| $Z$ | change of water level in surge tank, downward relative to initial level, m | $\alpha_T$ | head loss coefficient of throttling orifice, $s^2 \cdot m^{-5}$ |
| $h_H$ | head loss of headrace tunnel, m | $Q_P$ | discharge in penstock, $m^3 \cdot s^{-1}$ |

| | | | |
|---|---|---|---|
| $Q_H$ | discharge in headrace tunnel, $m^3 \cdot s^{-1}$ | $T_{wH}$ | flow inertia time constant of headrace tunnel, s |
| $h_P$ | head loss of penstock, m | $F$ | sectional area of surge tank, $m^2$ |
| $H$ | turbine head, m | $T_{WP}$ | flow inertia time constant of penstock, s |
| $M_t$ | kinetic moment, N·m | $e_{qh}$, $e_{qx}$, $e_{qy}$ | discharge transfer coefficients of turbine |
| $Y$ | guide vane opening, mm | $e_h$, $e_x$, $e_y$ | moment transfer coefficient of turbine |
| $N_t$ | turbine unit frequency, Hz | $T_a$ | turbine unit inertia time constant, s |
| $K_i$ | integral gain, $s^{-1}$ | $K_p$ | proportional gain |
| $e_g$ | load self-regulation coefficient | $\delta$ | power angle, rad |
| $E'$ | transient voltage of generator, p.u | $V_t$ | bus voltage of power grid, p.u |
| $x'_d$ | transient reactance of $d$ axis, p.u | $x_q$ | synchronous reactance of $q$ axis, p.u |
| $D_a$ | equivalent damping coefficient | $B$ | power conversion factor |
| $D_s$ | self-regulating coefficient of the equivalent load of power grid | $T_g$ | inertia time constant of the servomotor of power grid equivalent, s |
| $T_s$ | inertia time constant of power grid equivalent unit, s | $R_g$ | equivalent permanent difference coefficient of power grid |
| $f_r$ | basic power grid frequency, Hz | $\xi$ | intermediate state variable |
| $M_g$ | resisting moment, N·m | $t$ | time, s |
| $N_s$ | power grid frequency, Hz | $A(x_t)$ | amplitude of dynamic response of $x_t$ |
| $h$ | relative deviation value of $H$ | $g$ | acceleration of gravity, $m \cdot s^{-2}$ |
| $z$ | relative deviation value of $Z$ | $x_s$ | relative deviation value of $N_s$ |
| $q_H$ | relative deviation value of $Q_H$ | $y$ | relative deviation value of $Y$ |
| $q_P$ | relative deviation value of $Q_P$ | $m_t$ | relative deviation value of $M_t$ |
| $x_t$ | relative deviation value of $N_t$ | $m_g$ | relative deviation value of $M_g$ |

Note that: $Q_{P0} = Q_{H0} = Q_0$, $q_H = \frac{Q_H - Q_{H0}}{Q_{H0}}$, $z = \frac{Z}{H_0}$, $q_P = \frac{Q_P - Q_{P0}}{Q_{P0}}$, $h = \frac{H - H_0}{H_0}$, $m_t = \frac{M_t - M_{t0}}{M_{t0}}$, $m_g = \frac{M_g - M_{g0}}{M_{g0}}$, $x_t = \frac{N_t - N_{t0}}{N_{t0}}$, $x_s = \frac{N_s - N_{s0}}{N_{s0}}$, $y = \frac{Y - Y_0}{Y_0}$, $T_F = \frac{FH_0}{Q_{H0}}$. The subscript 0 refers to the initial value of corresponding variable.

## References

[1] Liu Y and Guo W C 2021 *Renew. Energ.* **171** 557–81
[2] Xu B B, Chen D Y, Venkateshkumar M, Xiao Y, Yue Y, Xing Y Q and Li P Q 2019 *Appl. Energy* **248** 446–62
[3] Liu Y and Guo W C 2022 *Int. J. Electr. Power Energy Syst.* **139** 107984
[4] Zhang H, Chen D Y, Xu B B, Wu C Z and Wang X Y 2017 *Nonlinear Dyn.* **87**(4) 2519–28
[5] Zhang H, Chen D Y, Xu B B, Wu C Z and Wang X Y 2018 *Commun Nonlinear Sci Numer Simul* **54** 136-47.
[6] Zhang J S, Xu B B, Chen D Y, Li H H and Zhang J J 2019 *Journal of Hydroelectric Engineering* **38**(4) 146–59
[7] Yuan X H, Chen Z H, Yuan Y B and Huang Y H 2015 *Energy* **93** 173–87
[8] Guo W C, Yang J and Yang J B 2019 *IOP Conf. Ser.: Earth Environ. Sci.* **240**(5) 052018
[9] Guo W C and Peng Z Y 2020 *Sustain. Energy Technol. Assess.* **40** 100777
[10] Hanselman D C and Littlefield B 2005 *Mastering Matlab 7* (New Jersey: Pearson/Prentice Hall)
[11] Xu X Y and Guo W C 2021 *Sustain. Energy Technol. Assess.* **44** 101088
[12] Bracewell R N and Bracewell R N 1986 *The Fourier Transform and Its Applications* (New York: McGraw–Hill)
[13] Saltelli A, Tarantola S and Chan K P S 1999 *Technometrics* **41**(1) 39–56
[14] Saltelli A and Bolado R 1998 *Comput. Stat. Data Anal.* **26**(4) 445–60